Interaction and Multiscale Mechanics, Vol. 1, No. 3 (2008) 381-396
DOI: http://dx.doi.org/10.12989/imm.2008.1.3.381

Wind-induced aerostatic instability of cable-supported bridges by a two-stage geometric nonlinear analysis

Y. B. Yang*

Department of Building and Construction, City University of Hong Kong, Tat Chee Avenue, Kowloon, Hong Kong

Jiunn-Yin Tsay‡

Department of Civil Engineering, National Taiwan University, Taipei, 10617, Taiwan

(Received August 17, 2007, Accepted August 17, 2008)

Abstract. The aerostatic instability of cable-supported bridges is studied, with emphasis placed on modeling of the geometric nonlinear effects of various components of cable-supported bridges. Two-node catenary cable elements, which are more rational than truss elements, are adopted for simulating cables with large or small sags. Aerostatic loads are expressed in terms of the mean drag, lift and pitching moment coefficients. The geometric nonlinear analysis is performed with the dead loads and wind loads applied in two stages. The critical wind velocity for aerostatic instability is obtained as the condition when the pitching angle of the bridge deck becomes unbounded. Unlike those existing in the literature, each intermediate step of the incremental-iterative procedure is clearly given and interpreted. As such, the solutions obtained for the bridges are believed to be more rational than existing ones. Comparisons and discussions are given for the examples studied.

Keywords: catenary cable; critical wind load; geometric nonlinear analysis; aerostatic instability; cable-supported bridge.

1. Introduction

The collapse of the Tacoma Narrows Bridge in 1940 evoked intensive research on the wind-induced instability of cable-supported bridges. The historical development and theories for the wind-induced effects on the stability of cable-supported bridges were well covered in the books by Simiu and Scanlan (1986), and Xiang (2005), wherein the wind-structure interaction is recognized as a key factor to the instability of long-span cable-supported bridges. The wind-induced instability can be categorized into the aerostatic instability (e.g., torsional divergence, torsional-flexural buckling) and aerodynamic instability (e.g., vortex shedding, galloping, flutter, buffeting). For each category of instability, a critical wind velocity can be solved of the bridge, which should not be exceeded during the service life of a properly designed bridge.

* Professor on leave from National Taiwan University, E-mail: ybyang@ntu.edu.tw
‡ Former Doctoral Student, E-mail: d93521017@ntu.edu.tw

Three components of static wind loads may occur on a bridge, i.e., the drag force, lift force and pitching moment, all of which are functions of the wind angle of attack. Whenever the critical wind speed is reached, static instability may occur in the form of *torsional divergence* or *lateral-torsional buckling*. The torsional divergence is characterized by a monotonic increase of the twist angle of the bridge deck to failure, and the lateral-torsional buckling by a combined flexural deformation and twist of the bridge deck, accompanied by a drop in the effective stiffness of the structure to zero.

The torsional divergence under the pitching moment has been studied by Simiu and Scanlan (1986). The lateral-torsional buckling was demonstrated by Hirai *et al*. (1967) to have occurred on a suspension bridge under the static wind loads in a wind tunnel test. By taking into account the effects of wind loads and geometric nonlinearity, a finite element approach was presented by Boonyapinyo *et al*. (1994) to calculate the critical wind velocity for the lateral-torsional buckling of cable-stayed bridges, using the beam element derived by Yang and McGuire (1986), in which the warping effect of the member cross sections was neglected. Further research along these lines includes those by Xiang *et al*. (2005), Cheng *et al*. (2000), and Zhang (2006).

This paper is focused on an accurate modeling of the geometric nonlinear effects of various components of cable-supported bridges and on an explicit expression of all the intermediate steps, along with physical meanings given, involved in the incremental-iterative analysis. The cables will be modeled by the two-node catenary cable elements, rather than the truss elements, which can be uniquely determined for given values of pretension force and unstressed length. The girders and pylons will be modeled by the beam elements with the instability effect of all kinds of actions taken into account.

To account for the effect of dead loads and wind loads, a two-stage geometric nonlinear analysis is performed. In the first stage of analysis, the dead loads are allowed to increase from zero to the full values. The effect of instability associated with the internal force distribution under the dead loads is represented by a geometric stiffness matrix. In the second stage of analysis, the dead loads are kept constant (so is the corresponding geometric stiffness matrix), while the wind loads are allowed to increase in an incremental manner. Again, the instability associated with the internal force distribution corresponding to the wind loads is represented by another geometric stiffness matrix. Considering the fact that the geometric stiffness matrix is a linear function of the member actions, the gross instability effects on the bridge due to both types of loadings can be represented by superposing the aforementioned two geometric stiffness matrices.

The generalized displacement control (GDC) method proposed by Yang and Shieh (1990) is adopted to solve the critical wind velocity for aerostatic instability, by which each term involved in the incremental-iterative procedure is physically explained. The critical wind velocity for aerostatic instability is obtained as the condition of divergence or when the pitching angle of the bridge deck becomes unbounded. The reliability of the analysis programs developed will be demonstrated in the analysis of the Kao-Ping-Hsi Bridge with a main span of 330 m, located in southern Taiwan, and another cable-stay bridge with a main span of 1000 m. Comparison will be made with existing results with discussions given.

2. Beam, truss and two-node catenary cable elements

Both the beam and truss elements adopted are those derived by Yang and Kuo (1994) considering the instability effects of all kinds of member actions. The stiffness matrix $[k]$ of the 12-degree-of-

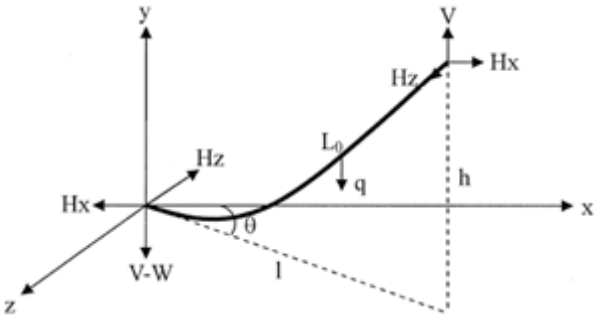

Fig. 1 Three-dimensional catenary cable element

freedom beam element is composed of two components, i.e., $[k] = [k_e] + [k_g]$, where $[k_e]$ is the *elastic stiffness matrix* and $[k_g]$ the *geometric stiffness matrix*, including the contribution of induced moment matrix given in Yang and Kuo (1994).

The truss element is only used for comparison with the two-node catenary cable element. As conventional, the equivalent modulus of elasticity used for the straight two-node truss element is

$$E_{eq} = \frac{E}{1 + \frac{w_c l AE}{12T^3}} \tag{1}$$

where E denotes the elastic modulus, A the cross-sectional area, l the horizontal projected length, w_c the weight per unit length, and T the tension force of the cable. For cables under the self weight only, the sag can be quite large. For cables subjected to large pretension, in addition to the self-weight, the sag may be quite small. The aforementioned equivalent truss element approach is not suitable for simulating cables in the natural shape, i.e., with zero pretension. For instance, by letting the pretension T equal to 0, one finds that the equivalent modulus E_{eq} also equals zero, which is physically not justified.

The two-node catenary cable element shown in Fig. 1 is adopted, by which both the *self weight* and *pretension* effects are taken into account. It is good for simulating cables with both large and small pretensions, or with small and large sags, respectively (Yang and Tsay 2007). This is an improvement over the equivalent truss element conventionally used in the analysis of cable-supported structures. The stiffness matrix $[k_c]$ of the cable element can be obtained directly as the inverse of the flexibility matrix as follows:

$$[k_c]_{6\times 6} = \begin{bmatrix} [k] & -[k] \\ -[k] & [k] \end{bmatrix} \tag{2}$$

where

$$[k] = [F]^{-1}_{3\times 3} = \begin{bmatrix} f_{11} & f_{12} & 0 \\ f_{21} & f_{22} & 0 \\ 0 & 0 & f_{33} \end{bmatrix}^{-1} \tag{3}$$

The coefficients f_{ij} in the flexibility matrix $[F]$ are obtained as the differentials of the horizontal and vertical projection lengths l, h of the cable, which are functions of the horizontal and vertical tension components H and V, i.e., $l = f(H, V)$, $h = g(H, V)$, namely,

$$f_{11} = \frac{\partial f}{\partial H} = \frac{L_0}{EA} + \frac{1}{q}\left[\sinh^{-1}\left(\frac{V}{H}\right) - \sinh^{-1}\left(\frac{V-W}{H}\right)\right] + \frac{1}{q}\left[-\frac{V}{\sqrt{H^2+V^2}} + \frac{V-W}{\sqrt{H^2+(V-W)^2}}\right] \quad (4a)$$

$$f_{12} = \frac{\partial f}{\partial V} = \frac{1}{q}\left[\frac{H}{\sqrt{H^2+V^2}} - \frac{H}{\sqrt{H^2+(V-W)^2}}\right] \quad (4b)$$

$$f_{21} = \frac{\partial g}{\partial H} = \frac{1}{q}\left[\frac{\sqrt{H^2+V^2}}{H} - \frac{\sqrt{H^2+(V-W)^2}}{H}\right] + \frac{1}{qH^2}\left[\frac{-V^2H}{\sqrt{H^2+V^2}} + \frac{(V-W)^2H}{\sqrt{H^2+(V-W)^2}}\right] \quad (4c)$$

$$f_{22} = \frac{\partial g}{\partial V} = \frac{L_0}{EA} + \frac{1}{q}\left[\frac{H}{\sqrt{H^2+V^2}} - \frac{V-W}{\sqrt{H^2+(V-W)^2}}\right] \quad (4d)$$

$$f_{33} = \frac{l}{H} = \frac{L_0}{EA} + \frac{1}{q}\left[\sinh^{-1}\left(\frac{V}{H}\right) - \sinh^{-1}\left(\frac{V-W}{H}\right)\right] \quad (4e)$$

Here, $q = W / L_0$, H is the horizontal component of the tension (which is constant everywhere since no axial loads are applied on the cable), V is the vertical reaction of the support, W the self weight of the cable, and L_0 the unstressed length of the cable (which is uniquely determined for a given pretension, as will be presented below).

3. Unstressed length of centenary cable

Unlike the truss element that requires the input of pretension force for structural analysis, the catenary cable element requires the input of the unstressed length L_0 of the cable instead. However, the unstressed length L_0 of each cable can be only determined by a trial-and-error procedure, as outlined below, prior to execution of structural analysis. First of all, the reaction forces H, V existing at the ends of each cable are obtained as the components of the pretension force T. The unstressed length L_0 can be related to the horizontal projection l of the cable as (Yang and Tsay 2007):

$$l = \frac{HL_0}{EA} + \frac{H}{q}\left[\sinh^{-1}\left(\frac{V}{H}\right) - \sinh^{-1}\left(\frac{V-W}{H}\right)\right] \quad (5)$$

We shall use this equation to compute the unstressed length L_0 of the cable. Here, the modulus of elasticity E, cross-sectional area A, and self weight q of the cable are all assumed to be known. Given the nodal coordinates of the two ends of the cable, both the horizontal projection l and the distance between the two end points can be computed. The latter will be used as the first trial value for the unstressed length L_0. By substituting this trial value into Eq. (5), an improved horizontal projection length l^* can be computed. Let Δl denote the difference between the given and computed projection lengths, i.e.,

$$\Delta l = l - l^* \quad (6)$$

If the difference Δl is less than a preset tolerance, then the unstressed length L_0 used is the solution desired. Otherwise, depending on whether Δl is positive or negative, a new trial value of

unstressed length L_0 larger or smaller than the previous trial value should be used, and the procedure should be repeated. Based on the above procedure, the unstressed length L_0 can be obtained for a cable with given pretension force T.

4. Dead load analysis

An aerostatic nonlinear analysis of cable-supported bridges consists of two stages. In the first stage, the bridge is subjected only to the *dead loads*, and in the second stage it is subjected to the *wind loads*. In this study, both stages will be solved in an incremental-iterative manner using the method proposed by Yang and Shieh (1990).

In order to consider the effect of geometry change, the dead loads will be assumed to be applied in an incremental way. The following are the equations of equilibrium for the bridge under the dead loads written specifically for the jth iteration of the ith increment:

$$[K_{j-1}^i]\{\Delta U_j^i\} = \Delta\lambda_j^i\{\hat{P}\} + \{R_{j-1}^i\} \tag{7}$$

where $[K_{j-1}^i]$ is the stiffness matrix of the system, $\{\hat{P}\}$ the reference dead loads, $\Delta\lambda_j^i$ the load increment parameter, $\{R_{j-1}^i\}$ the unbalanced forces, and $\{\Delta U_j^i\}$ the displacement increments generated during the jth iterative step. The stiffness matrix $[K]$ in Eq. (7) is composed of two parts, the *elastic stiffness matrix* $[K_e]$ and the *geometric stiffness matrix* $[K_g]$, i.e., $[K] = [K_e] + [K_g]$. The elastic stiffness matrix $[K_e]$ is assembled by looping over all the beam elements (for the girder and pylons) and cable elements, while the geometric stiffness matrix $[K_g]$, which is a linear function of the member actions, is assembled by looping over all the beam elements only, since the cable elements are always in tension and have nothing to do with geometric instability.

The *unbalanced forces* $\{R_{j-1}^i\}$ are computed as the differences between the *applied loads* $\{P_{j-1}^i\}$ and *resistant forces* $\{F_{j-1}^i\}$ existing at the *end* of the last iterative step,

$$\{R_{j-1}^i\} = \{P_{j-1}^i\} - \{F_{j-1}^i\} \tag{8}$$

where for $j = 1$, $\{R_{j-1}^i\} \equiv \{R_l^{i-1}\}$, $\{P_0^i\} \equiv \{P_l^{i-1}\} = \lambda_l^{i-1}\{\hat{P}\}$, and $\{P_0^i\} \equiv \{F_l^{i-1}\}$, with l indicating the *last* iteration of the last $(i-1)$ increment. For convenience, the structural equations in Eq. (7) can be decomposed into two parts,

$$[K_{j-1}^i]\{\Delta\hat{U}_j^i\} = \{\hat{P}\} \tag{9a}$$

$$[K_{j-1}^i]\{\Delta\overline{U}_j^i\} = \{R_{j-1}^i\} \tag{9b}$$

along with the displacement increments $\{\Delta U_j^i\}$ given as

$$\{\Delta U_j^i\} = \Delta\lambda_j^i\{\Delta\hat{U}_j^i\} + \{\Delta\overline{U}_j^i\} \tag{10}$$

By the *generalized displacement control* (GDC) method (Yang and Shieh 1990), the load increment $\Delta\lambda_1^i$ for the first iteration (i.e. for $j = 1$) of the ith incremental step is

$$\Delta\lambda_1^i = \Delta\lambda_1^1|GSP|^{1/2} \tag{11}$$

where $\Delta\lambda_1^i$ is the load increment for the 1st iteration of the 1st increment, which is given. The

generalized stiffness parameter (*GSP*) is defined as

$$GSP = \frac{\{\Delta\hat{U}_1^1\}^T\{\Delta\hat{U}_1^1\}}{\{\Delta\hat{U}_1^{i-1}\}^T\{\Delta\hat{U}_1^i\}} \tag{12}$$

For the remaining iterations, i.e., for $j \geq 2$,

$$\Delta\lambda_j^i = \frac{\{\Delta\hat{U}_1^{j-1}\}^T\{\Delta\overline{U}_j^i\}}{\{\Delta\hat{U}_1^{j-1}\}^T\{\Delta\hat{U}_j^i\}} \tag{13}$$

The *accumulated or total load parameter* up to the *j*th iteration of the *i*th incremental step is

$$\lambda_j^i = \lambda_{j-1}^i + \Delta\lambda_j^i \tag{14}$$

where for $j = 1$, $\lambda_{j-1}^i \equiv \lambda_l^{i-1}$. Main features of the GDC method are as follows: First, the load increments are adjusted as a function of the structural stiffness, as indicated by Eq. (11). Second, iterations are *not* performed at constant loads, i.e., the load parameter $\Delta\lambda_j^i$ is allowed to vary according to Eq. (13), to circumvent the numerical difficulty associated with iterations around the limit points. The *GSP* is a parameter related to the change in stiffness of the structure. It starts with $GSP = 1$ for the first increment ($i = 1$) and becomes negative only for the increments "immediately after" the limit points, while for the other increments, it is always positive. Such a feature serves as a good indicator for *reversing the loading direction* when passing a limit point.

The element displacements $\{\Delta u_j^i\}$ can be computed once the structural displacement increments $\{\Delta U_j^i\}$ are made available. With this, the element force increments $\{\Delta f_j^i\}$ can be computed by the concept of natural deformations. By superimposing the *initial* element forces $\{f_{j-1}^i\}$ existing prior to the *j*th iteration with the force increments $\{\Delta f_j^i\}$, the *total element forces* $\{f_j^i\}$ acting at the end of the *j*th iteration can be computed as

$$\{f_j^i\} = \{f_{j-1}^i\} + \{\Delta f_j^i\} \tag{15}$$

where the initial nodal forces $\{f_{j-1}^i\}$ are *directly included* since they are treated as forces acting along the axes of the deformed configuration. This is based on the rigid body rule, which requires the initial forces acting on a body in equilibrium to rotate following the rigid rotation of the body with no change in magnitude, so as to preserve the equilibrium of the body in the deformed configuration (Yang and Chiou 1987, Yang *et al*. 2007).

Meanwhile, one can proceed to update the geometry, i.e., the nodal coordinates, element axes and lengths, of the structure using the displacement increments $\{\Delta U_j^i\}$. Based on the updated geometry and element forces $\{f_j^i\}$ of the structure, the *total resistant forces* $\{F_j^i\}$ acting at each node of the structure for the *j*th iteration can be computed. It follows that the *unbalanced forces* $\{R_j^i\}$ existing at the *end* of the *j*th iteration are

$$\{R_j^i\} = \{P_j^i\} - \{F_j^i\} = \lambda_j^i\{\hat{P}\} - \{F_j^i\} \tag{16}$$

If the unbalanced forces $\{R_j^i\}$ are greater than preset tolerance using proper definitions, then another iteration starting with the solution of Eq. (9) by setting $j = j + 1$ should be repeated. In this

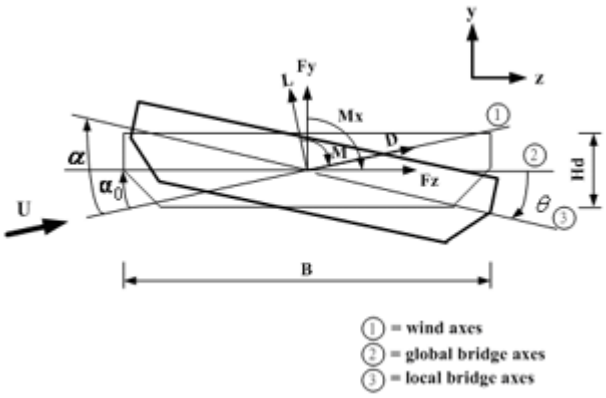

Fig. 2 Aerostatic wind loads acting on the deck and related axes

connection, the elastic stiffness matrix $[K_e]$ should be updated to reflect the change in element lengths, and the geometric stiffness matrix $[K_g]$ should be updated to reflect the change in element forces $\{f_j^i\}$. Once the convergent solution is obtained for the current incremental step, one can set $i = i + 1$ and proceed to the next incremental step beginning with Eq. (9).

5. Wind load analysis

The static wind loads are displacement-dependent in that they will cause deformations on the bridge, and will also be affected by the change in the angle of inclination of the bridge deck due to deformations. The static wind loads, i.e., drag D, lift L, and pitching moment M, per unit length of the span of the bridge can be related to the coefficients C_D, C_L, C_M, respectively, as functions of the wind angle of attack, that is,

$$D = \frac{1}{2}\rho U^2 H_d C_D \tag{17a}$$

$$L = \frac{1}{2}\rho U^2 B C_L \tag{17b}$$

$$M = \frac{1}{2}\rho U^2 B^2 C_M \tag{17c}$$

where ρ is the air density, U the mean wind velocity, B the bridge deck width, and H_d the projected height of the bridge deck against the wind flow (see Fig. 2). Conventionally, the coefficients C_D, C_L, C_M obtained from the wind tunnel test have been expressed in the local wind axes. The wind forces can be transformed to the global axes of the bridge as follows (Boonyapinyo *et al*. 1994):

$$F_y = \frac{1}{2}\rho U_r^2 B C_y \tag{18a}$$

$$F_z = \frac{1}{2}\rho U_r^2 H_d C_z \tag{18b}$$

$$M_x = \frac{1}{2}\rho U_r^2 B^2 C_x \tag{18c}$$

where

$$C_y(\alpha) = \left[C_L(\alpha) + C_D(\alpha)\frac{H_d}{B}\tan\alpha_0\right]\sec\alpha_0 \tag{19a}$$

$$C_z(\alpha) = \left[C_D(\alpha) - C_L(\alpha)\frac{B}{H_d}\tan\alpha_0\right]\sec\alpha_0 \tag{19b}$$

$$C_t(\alpha) = C_M(\alpha)\sec^2\alpha_0 \tag{19c}$$

and

$$U_r = U\cos\alpha_0 \tag{20}$$

The wind loads F_y, F_z, M_x and the coefficients C_y, C_z, C_t should be interpreted as those defined in the global axes, U_r is the relative wind velocity in the global axes, α_0 is the *initial angle of attack*, i.e., the angle between the wind direction and the bridge deck line after the dead load analysis, as shown in Fig. 2, and α is the *effective wind angle of attack*, which is equal to α_0 plus the torsional displacement θ of the deck.

After the first stage of analysis, the *internal resistant forces*, denoted as $\{F\}_D$, corresponding to the *dead loads*, denoted as $\{P\}_D$, was developed on the bridge. The effect of instability caused by such internal forces $\{F\}_D$ on the bridge is represented by the geometric stiffness matrix $[K_g]_D$, where the subscript D signifies the dead loads. In the second stage of analysis involving the wind loads, the geometric stiffness matrix $[K_g]_D$ caused by the dead loads is regarded as the *initial stiffness matrix*. The wind loads will induce additional displacements and internal forces on the bridge. The additional displacements will cause further change in geometry of the bridge, for which the elastic stiffness matrix $[K_e]$ has to be updated accordingly. The additional internal forces will add potential of instability to the bridge, which can be represented by including another geometric stiffness matrix $[K_g]_W$ as a function of the additional internal forces.

One particular problem with the wind loads analysis is that for a given wind velocity U, the wind loads F_x, F_z M_x calculated from Eq. (18) are functions of the coefficients C_y, C_z, C_t, which in turn are functions of the effective angle α of attack of the wind. The effective angle α of attack is known only when the deformed shape of the bridge under the specified wind loads is known. Such a problem can be resolved by the incremental-iterative procedure described below. First, we shall assume a wind velocity increment ΔU for each increment and set the effective angle α of attack equal to the initial angle α_0 for starting. In the iterative process, this angle is updated to reflect the change in the twist angle of the bridge deck, so are the wind loads.

As for the wind load analysis, we shall use m to denote an incremental step, and n an iterative step within the incremental step. Let us increase the wind velocity U by an amount ΔU at each incremental step. The total wind velocity at the mth incremental step is

$$U = m \cdot \Delta U \tag{21}$$

Given the wind velocity U for the mth increment, the per-unit-length wind loads F_x, F_z M_x can be calculated from Eq. (18) using the updated, deformed shape of the bridge obtained from the last $(n-1)$ iteration. Let us use $\{W_n^m\}$ to denote the *total wind loads* at the nth iteration of the mth increment, based on the effective angle α of attack available. The *wind load increment* $\{\Delta W_n^m\}$ for the mth incremental step can be expressed as

$$\{\Delta W_n^m\} = \{W_n^m\} - \{W_{n-1}^m\} \tag{22}$$

Accordingly, the governing equation for the *n*th iteration of the *m*th increment for the bridge under the wind loads is

$$[K_{n-1}^m]\{\Delta U_n^m\} = \{\Delta W_n^m\} + \{R_{n-1}^m\} \tag{23}$$

where $\{\Delta U_n^m\}$ denotes the displacement increments generated at the *n*th iteration and $\{R_{n-1}^m\}$ the unbalanced forces. The structural stiffness matrix $[K]$ in Eq. (23) should be computed as

$$[K] = [K_e] + [K_g]_D + [K_g]_W \tag{24}$$

where all quantities are those existing at the *beginning* of the *n*th iteration, $[K_g]_D$ is the geometric stiffness matrix associated with the dead loads, which is kept constant throughout the wind load analysis.

The elastic stiffness matrix $[K_e]$ should be updated at each iteration to reflect the change in geometry of the bridge, i.e., the change in length of each element. The geometric stiffness matrix $[K_g]_W$ is a linear function of the *internal forces* $\{F_{n-1}^m\}$ caused by the *wind loads*. It should be noted that the instability effects caused by the dead loads and wind loads are treated by different geometric stiffness matrices, simply because they are linear functions of the member actions and therefore their gross effect can be obtained simply by superposition of the separate effects (Yang and Kuo 1994, Yang *et al*. 2007).

The unbalanced forces $\{R_{n-1}^m\}$ in Eq. (23) are computed as the difference between the *total applied loads* $\{P_{n-1}^m\}_T$ and the *total resistant forces* $\{F_{n-1}^m\}_T$ of the bridge, that is,

$$\{R_{n-1}^m\} = \{P_{n-1}^m\}_T - \{F_{n-1}^m\}_T \tag{25}$$

Here, the total applied loads $\{P_{n-1}^m\}_T$ are composed of two parts,

$$\{P_{n-1}^m\}_T = \{P\}_D + \{W_{n-1}^m\} \tag{26}$$

where $\{P\}_D$ denotes the total dead loads and $\{W_{n-1}^m\}$ the total wind loads increment. The total internal forces $\{F_{n-1}^m\}_T$ are

$$\{F_{n-1}^m\}_T = \{F\}_D + \{F_{n-1}^m\} \tag{27}$$

where $\{F\}_D$ denotes the internal forces caused by the dead loads and $\{F_{n-1}^m\}$ the internal forces caused by the wind loads. The following are the initial conditions for the terms appearing in Eqs. (25)-(27):

$$\{P_0^m\}_T \equiv \{P_l^{m-1}\}_T \tag{28a}$$

$$\{F_0^m\} \equiv \{F_l^{m-1}\} \tag{28b}$$

$$\{W_0^m\} \equiv \{W_l^{m-1}\} \tag{28c}$$

$$\{F_0^m\}_T \equiv \{F_l^{m-1}\}_T \tag{28d}$$

where the subscript *l* indicates the last iteration.

For the present purposes, the structural equations in Eq. (23) for the *n*th iteration of the *m*th

increment can be decomposed into two parts as

$$[K_{n-1}^m]\{\Delta\hat{U}_n^m\} = \{\Delta W_n^m\} \tag{29a}$$

$$[K_{n-1}^m]\{\Delta\overline{U}_n^m\} = \{R_{n-1}^m\} \tag{29b}$$

together with the displacement increments $\{\Delta U_n^m\}$ caused by the *wind loads* given as

$$\{\Delta U_n^m\} = \{\Delta\hat{U}_n^m\} + \{\Delta\overline{U}_n^m\} \tag{30}$$

Using the displacement increments $\{\Delta U_n^m\}$, the element displacement increments $\{\Delta u_n^m\}$ can be computed. In accordance, the element force increments $\{\Delta f_n^m\}$ can also be computed by the concept of natural deformations. By superimposing the *initial* element forces $\{f_{n-1}^m\}$ existing prior to the nth iteration with the force increments $\{\Delta f_n^m\}$, the *total element forces* $\{f_n^m\}$ acting at the end of the nth iteration can be computed as

$$\{f_n^m\} = \{f\}_D + \{f_{n-1}^m\} + \{\Delta f_n^m\} \tag{31}$$

Here, $\{f\}_D$ are the internal forces caused by the dead loads, which remain constant throughout the second stage of analysis, both $\{f\}_D$ and initial nodal forces $\{f_{n-1}^m\}$ are *directly included* in the superposition according to the rigid body rule (Yang and Chiou 1987).

Meanwhile, one can proceed to update the geometry, i.e., nodal coordinates, element axes and lengths, of the structure using the displacement increments $\{\Delta U_n^m\}$. As the effective angle α of attack has been made available for the bridge deck, the wind coefficients C_y, C_z, and C_t can be determined and the total wind loads $\{W_n^m\}$ existing at the *end* of the nth iteration can be computed accordingly.

Based on the updated geometry and updated element forces $\{f_n^m\}$ of the structure, the *total resistant forces* $\{F_n^m\}$ acting at each node of the structure can be computed for the *end* of the nth iteration. It follows that the *unbalanced forces* $\{R_n^m\}$ existing at the *end* of the nth iteration are

$$\{R_n^m\} = \{W_n^m\} - \{F_n^m\} \tag{32}$$

If the unbalanced forces $\{R_n^m\}$ are greater than preset tolerance by proper definitions, then another iteration starting with the solution of Eq. (23) with $n = n + 1$ should be repeated. In this connection, the elastic stiffness matrix $[K_e]$ should be updated to reflect the change in element lengths, and the geometric stiffness matrix $[K_g]_W$ should be updated to reflect the variation of the total element forces caused by the winds, which are equal to $(\{f_{n-1}^m\} + \{\Delta f_n^m\})$, according to Eq. (31).

After an incremental step is completed, the wind speed U will be increased by the amount ΔU and the whole procedure of iteration as described above should be repeated for the next incremental step by setting $m = m + 1$. The critical wind speed U_{cr} is determined as the condition of divergence or when the pitching angle of the bridge deck approaches infinity or becomes unbounded in the sense of divergence.

6. Numerical examples

Five examples will be studied to demonstrate the reliability and applicability of the aerostatic

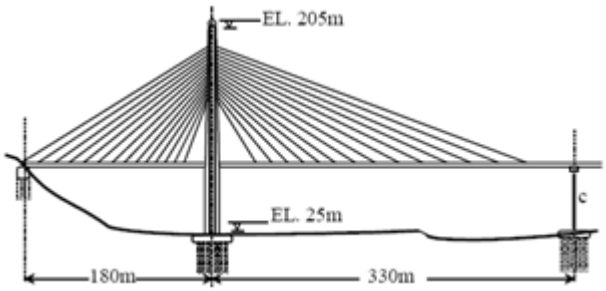

Fig. 3 Layout of Kao-Ping-Hsi Bridge (unit: m)

Table 1 Material and section properties of Kao-Ping-Hsi Bridge

Property	E (KN/m^2)	A (m^2)	I_y / I_z / J (m^4)	m (kg/m^3)	I_m (kg-m^2/m^3)
Main span	2.1×10^8	1.742	170.4/2.947/9.785	14150	142915
Side span	2.8×10^7	21.597	1533./32.608/98.1	3190	32219
Pylon	2.8×10^7	15.126 ~ 34.937	Varied	2550	Varied
Cable	1.85×10^8	0.012 ~ 0.0546	0	8830	0

Table 2 Results and comparison for Kao-Ping-Hsi Bridge (unit: Hz)

Frequency	f_1	f_2	f_3	f_4	f_5
Present study	0.261	0.511	0.648	0.674	0.757
DMI (1993a,b)	0.231	0.451	0.563~0.584	0.572	0.698
Cheng (2002)	0.275	0.520	0.640	0.650	0.740

instability analysis program developed for the cable-supported structures in this study. The results obtained will be compared with those existing in the literature. The following investigation is conducted primarily for the Kao-Ping-Hsi Bridge located in southern Taiwan, an asymmetric cable-stayed bridge with single inversed-Y pylon, single plane cable system, a deck width of 34.5 m and depth of 3 m, a steel main span of 330 m, and a concrete side span of 180 m (see Fig. 3). The wind-tunnel test of the section model and full bridge model with a scale of 1:80 and 1:150, respectively, were conducted by the boundary-layer wind tunnel of the Danish Maritime Institute (DMI 1993a,b), from which the mean static loads and aerodynamic derivatives have been determined accordingly.

The entire structure is modeled by a three-dimensional finite element model with a total of 116 nodes, 115 beam elements for the girder, pylon, and pier, and 28 catenary cable elements for the stay cables. The fish-bone structure of the girder is also simulated in the finite element model. The material and section properties of the major components of the bridge are listed in Table 1.

Example 1 – The first example is to compare the first five natural frequencies computed for the Kao-Ping-Hsi Bridge with those obtained experimentally by the DMI (1993a,b) and Cheng *et al.* (2002). As can be seen from Table 2, the natural frequencies computed for this model using the stiffness and mass matrices are close to the site measurement (Cheng *et al.* 2002), but are higher

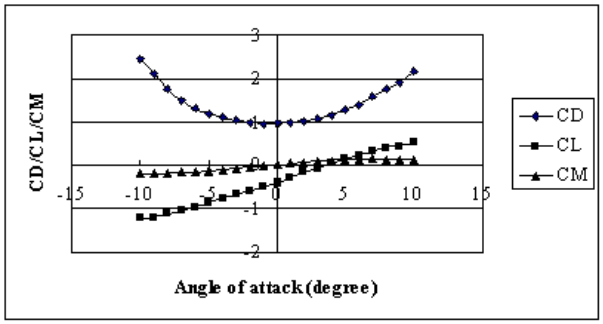

Fig. 4 Aerostatic coefficients C_D, C_L, C_M

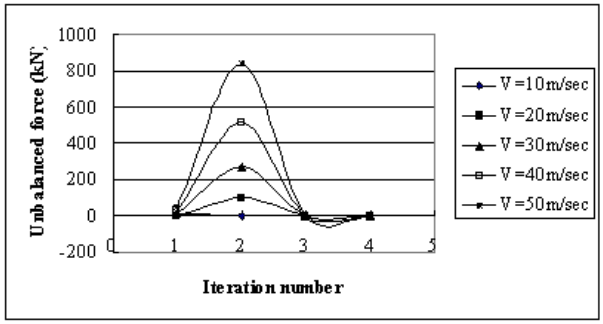

Fig. 5 Iteration number versus norm of unbalanced forces at different wind speeds

than those from the wind tunnel test. The natural frequencies presented herein are essential to computation of the aerostatic critical wind velocity for the Kao-Ping-Hsi Bridge to be shown in Example 3.

Example 2 – The second example is to demonstrate the convergence characteristics of the present procedure in the aerostatic instability analysis. One simply supported girder with a span of 330 m is studied with the same material and section properties as those of the Kao-Ping-Hsi Bridge. The aerostatic coefficients of the lift (C_D), drag (C_L) and pitching moment (C_M) have been determined for the incoming wind with the flow angle varying from -10^o to -10^o by an increment of 1^o in the DMI report (1993a) (Fig. 4). The iteration number versus the norm of the unbalanced forces at different wind speeds, i.e., from 10 to 50 m/s, has been plotted in Fig. 5. As can be seen, for the bridge subjected to winds at different speeds, rather accurate results can be obtained using an iteration number of three to four, as the norm of the unbalanced forces almost reduces to zero for each of the wind speeds considered. This is an indication of the efficient and convergent characteristics of the procedure proposed herein for evaluation of the aerostatic instability of cable-supported bridges.

Example 3 – The third example is to study the aerostatic critical wind speed for the Kao-Ping-Hsi Bridge described above. An indication of the onset of aerostatic instability was identified by the DMI (1993a) as either the condition of divergence or when the root mean square (r.m.s.) pitching

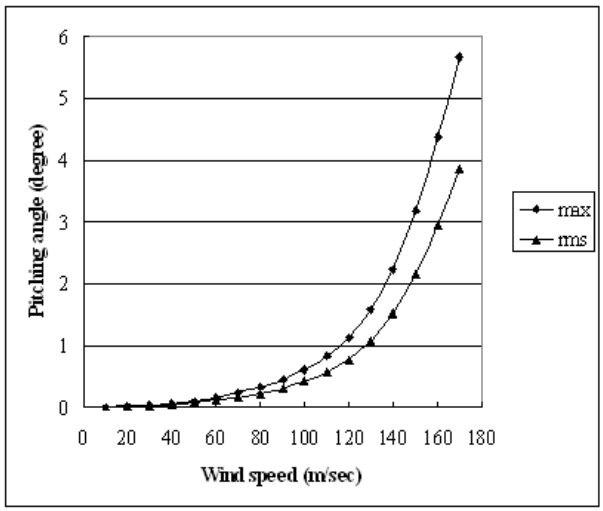

Fig. 6 Maximum and r.m.s. pitching angles of the deck vs. wind speed

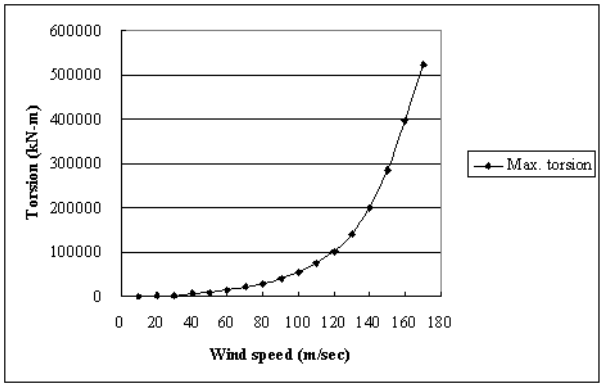

Fig. 7 Maximum torsional action of girder vs. wind speed

angle of the bridge deck becomes greater than 2°. In the present analysis, the wind speed has been increased from 10 to 170 m/s by an increment of 10 m/s. The maximum and r.m.s. pitching angles versus the wind speed solved for the bridge using the incremental-iterative procedure presented above have been plotted for the bridge in Fig. 6. From this figure, the critical wind speed for aerostatic instability can be identified as 149 m/s, since the r.m.s. pitching angle of the bridge deck exceeds 2° at that wind speed. Such a result is close to the critical wind speed of 140 m/s predicted by the DMI based on the same criterion (i.e., r.m.s. pitching angle of greater than 2°). In the meantime, the maximum torsional action of the girder also reveals the same characteristics of divergence under the critical wind speed in Fig. 7.

Example 4 – The fourth example is to investigate the effect of cable modeling on aerostatic instability of cable-supported bridges using the conventional equivalent truss elements and the two-node catenary cable elements. The three-span cable-stayed bridge (with span lengths of 450 + 1000

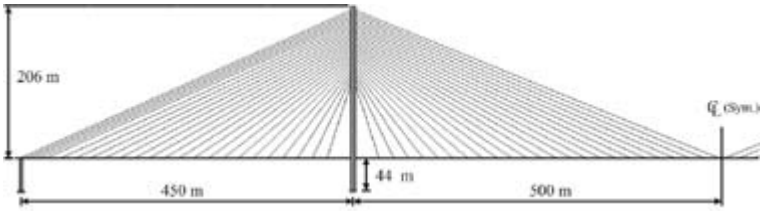

Fig. 8 Three-span cable-stayed bridge with 1000 m span

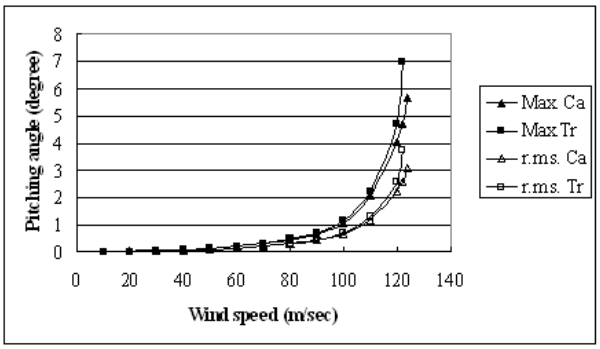

Fig. 9 Pitching angle of the deck vs. wind speed for models using different cable elements (Tr = Truss element, Ca = Catenary cable element)

+ 450 m) studied by Boonyapinyo *et al*. (1994) will be adopted herein (Fig. 8). For this example, the material and cross-sectional properties of the structural members are available in Hoshino and Miyata (1990). The entire structure is modeled by a three-dimensional finite element model that has a total of 127 nodes, 126 beam elements for the girder, pylon and pier, and 48 cable elements for the stay cables. The aerostatic coefficients are assumed to be identical to those of the Kao-Ping-Hsi Bridge.

The pitching angles of the bridge deck solved for the 1000 m bridge using the catenary cable elements and equivalent truss elements have been plotted with respect to the wind speed in Fig. 9. The critical wind speed obtained by the model with catenary cable elements is 124 m/s, slightly higher than the value of 122 m/s for the model using the equivalent truss elements. Evidently, the model with catenary cable elements shows relatively higher stiffness in resisting the pitching rotation at the same wind speed in comparison with the one using the equivalent truss element. In particular, we shall compare the forces existing in the shortest cable No. 13 (with unstressed length $L_0 = 125.81$ m) and the longest cable No. 23 (with unstressed length $L_0 = 500.62$ m), for which the unstressed length used for the catenary element is equivalent to the pretension force used for the equivalent truss element at the deck end. In other words, an initial pretension force of 12,050 kN (corresponding to unstressed length $L_0 = 125.81$ m) and 25,780 kN (corresponding to unstressed length $L_0 = 500.62$ m) are applied to cables No. 13 and No. 23, respectively, which equal approximately 25% of the ultimate strength of the cable.

As can be seen from Fig. 10, significantly smaller tension forces are obtained for the two cables using the catenary cable elements than the truss elements for the range of wind speeds considered. For instance, near the divergent wind speed of 121 m/s, a tension force of 20,236 kN and 14,250 kN

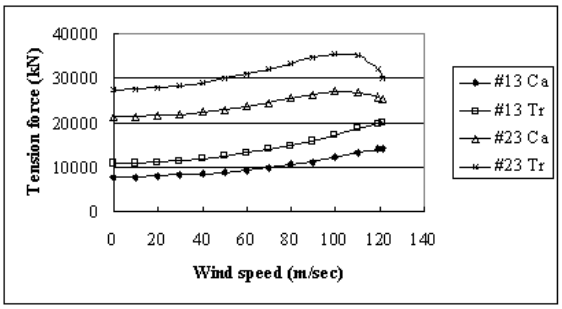

Fig. 10 Tension forces vs. wind speed for models using different cable elements (Tr = Truss element, Ca = Catenary cable element)

is computed for cable No. 13 using the equivalent truss elements and catenary cable elements, respectively. Meanwhile, a tension force of 30,131 kN and 25,350 kN is obtained for cable No. 23 using the equivalent truss elements and catenary cable elements, respectively.

7. Concluding remarks

The aerostatic instability of cable-supported bridges has been investigated by taking into account the effects of geometric nonlinearity and wind-structure interaction. The cables are modeled by the two-node catenary cable elements, by which the sag effect can be accurately taken into account, and the girders and pylons by the beam elements, by which the instability effect associated with all kinds of member actions are duly considered. The geometric nonlinear analysis is performed with the dead loads and wind loads applied in two stages. The critical wind velocity for aerostatic instability is obtained as the condition of divergence or when the pitching angle of the bridge deck becomes greater than a preset value. Each intermediate step of the incremental-iterative procedure is clearly given and interpreted. Due to the rigorous procedure adopted herein, the solutions obtained for the bridges are believed to be more rational than existing ones.

The present programs have been adopted in the solutions of two cable-stayed bridges on the assessment of aerostatic instability. Through comparison with previous results, the applicability of the programs in simulating cable-supported bridges is confirmed. With regard to the use of catenary cable elements, it was demonstrated that slightly higher critical wind speeds are obtained for the bridge studied, while substantially smaller tension forces are observed for the bridge cables for the range of wind speeds considered, compared with the use of equivalent truss elements.

Acknowledgement

The research works reported herein have been conducted as the result of a series of research projects granted by the National Science Council to the senior author, including NSC95-2221-E-002-314.

References

Agar, T.J.A. (1989), "Aerodynamic flutter analysis of suspension bridges by a modal technque", *Eng. Struct.*, **11**(2), 75-82.

Boonyapinyo, V., Yamada, H. and Miyata, T. (1994), "Wind-induced nonlinear lateral-torsional buckling of cable-stayed bridges", *J. Struct. Eng.*, ASCE, **120**(2), 486-506.

Chen, X., Matsumoto, M. and Kareem, A. (2000), "Aerodynamics coupling effects on flutter and buffeting of bridges", *J. Eng. Mech.*, **126**(1), 17-26.

Cheng C.C., Cherng R.H. and Zhang J.S. (2002), "The regular monitor control for statbility on Kao-Ping-Hsi Bridge", *The 6th National Conference on Structural Engineering,* Pingtung, August, No. J07, (in Chinese).

Cheng, J., Xiao, R.C. and Xiang, H.F. (2000), "Full range nonlinear analysis for long-span suspension bridge", *J. of Tongi University*, Shanghai, China, **28**(6), 717-720 (in Chinese).

Danish Maritime Institute (1993a), "Wind-tunnel tests for Kao-Ping-Hsi Bridge: Section model test", Report by Vienna Consulting Engineers to CECI, Taipei, Taiwan, R.O.C.

Danish Maritime Institute (1993b), "Wind-tunnel tests for Kao-Ping-Hsi Bridge: Full model test", Report by Vienna Consulting Engineers to CECI, Taipei, Taiwan, R.O.C.

Hirai, A. Okauchi, I., Ito, M., and Miyata T. (1967), "Studies on the critical wind velocity for suspension bridges", *Proc. Int. Res. Seminar on Wind Effects on Buildings and Sturctures*, University of Toronto Press, Ontario, Canada, 81-103.

Hoshino M. and Miyata, T. (1990), "Design trial of a long-span cable-stayed bridge with center span length of 1000 m", *Bridge Foundation Eng.*, **24**(2), 15-22 (in Japanese).

Ge, Y.J. and Tanaka, H. (2000), "Aerodynamic flutter analysis of cable-supported bridges by multi-mode and full-mode approaches", *J. Wind Eng. Ind. Aerodyn.*, **86**, 123-153.

Simiu, E. and Scanlan, R.H. (1986), *Wind Effects on Structures: Fundamentals and Applications to Design*, 2d ed., John Wiley and Sons, New York, N.Y.

Singh, L., Jones, N.P., Scanlan, R.H. and Lorendeaux, O. (1996), "Identification of lateral flutter derivatives of bridge decks", *J. Wind Eng. Ind. Aerodyn.*, **60**, 81-89.

Xiang, H.F. (2005), *Modern Theory and Practice on Bridge Wind Resisteance*, China Communications Press, Beijing, China (in Chinese).

Yang, Y.B. and Chen, C.H. (1998), "Three-dimensional aeroelastic stability analysis of cable-stayed bridges", *J. Chinese Inst. of Civil and Hydraulic Eng.*, **10**(3), 525-535. (in Chinese)

Yang, Y.B. and Chiou, H.T. (1987), "Rigid Body Motion Test for Nonlinear Analysis with Beam Elements," *J. Eng. Mech.*, ASCE, **113**(9), 1404-1419.

Yang, Y.B. and Kuo, S.R. (1994), *Theory and Analysis of Nonlinear Framed Structures*, Prentice Hall, Singapore.

Yang, Y.B., Lin, S.P. and Leu, L.J. (2007), "Solution Strategy and Rigid Element for Nonlinear Analysis of Elastically Structures Based on Updated Lagrangian Formulation", *Eng. Struct.*, **29**(6), 1189-1200.

Yang, Y.B., Mac, S.V. and Chen, C.H. (2001), "Multi-mode coupled buffeting analysis of cable-stayed bridges," *Int. J. Struct. Stability Dyn.*, **1**(3), 429-453.

Yang, Y.B. and McGure, W. (1986), "Stiffness matrix for geometric nonlinear analysis," *J. Struct. Eng.*, ASCE **112**(4), 853-877.

Yang, Y.B. and Shieh, M.S. (1990), "Solution method for nonlinear problems with multiple critical points", *AIAA J.*, **28**(12), 2110-2116.

Yang, Y.B. and Tsay, J.Y. (2007), "Geometric nonlinear analysis of cable structures with a two-node cable element by generalized displacement control method", *Int. J. Struct. Stability Dyna*, **7**(4), 571-588.

Zhang, X.J. (2006), "Advanced aerostatic analysis of long-span suspension bridges", *J. Zhejiang University Science A*, Hangzhou, China, **7**(3), 424-429.